RSC Advances

ROYAL SOCIETY OF CHEMISTRY

www.rsc.org/advances

Journal Name

ARTICLE

Fabrication of core@spacer@shell $Au_{nanorod}$@$mSiO_2$@Y_2O_3:Er nanocomposites with enhanced upconversion fluorescence

Received 00th January 20xx,
Accepted 00th January 20xx

DOI: 10.1039/x0xx00000x

www.rsc.org/

Huiqin Li,[ab] Qingqing Deng,[a] Bin Liu,[a] Jianhui Yang*[a] and Biao Wu*[a]

Herein, we report the fabrication of well-defined $Au_{nanorod}$@$mSiO_2$@Y_2O_3:Er nanocomposites with Au nanorod core, Y_2O_3:Er shell, and mesoporous silica as spacer. The thickness of mesoporous silica layer could be simply controlled by varying the reaction time and the amount of silica precursor. The nanocomposites were characterized by X-ray diffraction, transmission electron microscopy and Uv-vis absorption spectroscopy. Thanks to the two distinct plasmon absorptions of Au nanorod associated with the longitudinal and transverse surface plasmon resonances modes, the plasmon resonances matched very well to the absorption and emission wavelengths of Y_2O_3:Er in the near IR and visible regions, respectively. The strongest enhancement is observed when the optimized silica thickness is around 40 nm, resulting in about 10- and 8-fold enhancement for green and red emissions, respectively. Besides the enhanced upconversion fluorescence, the prepared nanocomposites with unique properties and functions offered by Au nanorod and mesoporous silica structure will expected to be useful in photothermal therapy, drug delivery, medical diagnostics and therapy.

1 Introduction

Lanthanide-doped upconversion nanocrystals have attracted intensive attention in recent year due to their unique optical properties and attractive potential applications in bioimaging, therapies, detection, lighting and second excitation sources.[1-3] It is known that the upconversion refers to absorb two or more low-energy photons (typically near infrared) and emit photons of higher energy (usually visible).[4] Compared with conventional fluorescent organic dyes and semiconductor nanocrystals, lanthanide-doped upconversion nanocrystals display obvious advantages, including low toxicity, sharp emission peaks, long emission lifetimes, and higher photochemical stability.[5] Moreover, the near infrared excitation wavelength was located at the "biological window" with the long penetration depth and low radiation damage in biological tissues benefit to bioimaging, biolabeling, and photodynamic therapy.[6,7] However, the quantum efficiency is usually low because of the small absorption cross sections of excited light. Therefore, it is still a challenge to improve the quantum efficiency of lanthanide-doped nanocrystals for their bio-applications in future.

Several approaches are used to enhance upconversion luminescence in lanthanide-doped nanocrystals, such as host lattice manipulation, energy transfer modulation, surface passivation, surface plasmon coupling, broadband sensitization, and photonic crystal engineering.[8,9] In concert with these approaches, plasmon modulation of upconversion is an efficient strategy to enhance the luminescent intensity of lanthanide-doped nanocrystals.[10,11] The origin of fluorescence enhancement is due to the enhanced electromagnetic field of surface plasmon resonances (SPR), which may lead to increase excitation and emission rate by the local field enhancement effect and surface plasmon coupled emission, respectively.[12-14] The quenching will reduce the efficiency by nonradiative energy transfer from the upconversion nanocrystal to the surface of plasmonic material.[15] The nonradiative relaxation can be abated by introducing a dielectric layer (silica) between them.[16-19] It is well known that noble metal gold (Au) and silver (Ag) nanoparticles show strong SPR, which are the most extensively studied plasmonic materials for upconversion enhancement.[20-22] Among various upconversion nanomaterials, yttrium oxide (Y_2O_3) is a well-known host material for upconversion because of its broad transparency, high refractive index, low phonon energy and high chemical stability.[23] Trivalent erbium (Er^{3+}) is an excellent candidate as activator populated tunable green and red emissions via energy-transfer upconversion and excited-state absorption processes under 980 nm excitation.[24] In 2010, Stucky et al. fabricated Ag@SiO_2@Y_2O_3:Er nanostructures with tuning of the upconversion fluorescence for bioimaging.[25] In 2013, Liu et al. reported the distance dependent of Au enhanced upconversion luminescence in Au/SiO_2/Y_2O_3:Yb^{3+},Er^{3+} nanoparticles.[26] The green emission was selectively enhanced due to the better spectral overlap with the Plasmon resonance of nanoparticles in the region of 500-550 nm. Au nanoshell was also used for enhanced upconversion fluorescence due to

[a]Key Laboratory of Synthetic and Natural Functional Molecule Chemistry (Ministry of Education), Shaanxi Key Laboratory of Physico-Inorganic Chemistry, College of Chemistry & Materials Science, Northwest University, Xi'an 710069, P. R. China. E-mail: jianhui@nwu.edu.cn, wubiao@nwu.edu.cn; Tel and Fax: +86-29-81535026.
[b]College of Chemistry & Chemical Engineering, Baoji University of Arts & Sciences, Baoji 721013, P. R. China.

its strong absorption in near infrared region increasing the excited flux.[27,28] Au nanorod displays two absorption peaks, which are respectively corresponding to a transverse plasma resonance in visible region and a longitudinal plasmon resonance in near infrared to infrared region.[29] However, most previous reports were focused on spherical Au/Ag nanostructures for the upconversion enhancement and there is no report about Au nanorod used for upconversion enhancement of lanthanide doped Y_2O_3. In view of gold nanorod with higher absorption cross-section and relatively light scattering efficiencies, we hypothesize achieve the simultaneous enhancement of emission and absorption in presence of Au nanorod.[30,31]

In this work, we describe a facile strategy for the fabrication of $Au_{nanorod}@mSiO_2@Y_2O_3$:Er nanocomposites with Au nanorod core, Y_2O_3:Er shell, and mesoporous silica as spacer. The thickness of mesoporous silica layer could be simply controlled by varying the reaction time and the amount of silica precursor. A 10- and 8-fold upconversion enhancement for green and red emissions is obtained by optimizing the thickness of mesoporous silica is around 40 nm. It is expected that the resulting nanocomposites could realize in upconversion imaging and therapy in biomedical fields.

2 Experimental section

Chemicals

Yttrium oxide (Y_2O_3, 99.99%), erbium oxide (Er_2O_3, 99.99%), chlorate gold ($HAuCl_4$), silver nitrate ($AgNO_3$), sodium borohydride ($NaBH_4$), ascorbic acid (Vc), cetyltrimethylammonium bromide (CTAB), tetraethyl orthosilicate (TEOS), Urea, ethanol, HCl (37%), HNO_3 and NaOH were purchased from Beijing Chemical Reagents Factory and were used as supplied without further purification. Deionized (DI) water was used in all experiments.

The stock solutions of $Y(NO_3)_3$ and $Er(NO_3)_3$ were synthesized by dissolving Y_2O_3 and Er_2O_3 in concentrated HNO_3 under heating with agitation and followed by evaporating the solvent.

Synthesis of $Au_{nanorod}@SiO_2@Y_2O_3$:Er nanocomposties

The Au nanorod was firstly synthesized using seeded growth method.[32] Briefly, 0.25 mL of $HAuCl_4$ (10 mmol•L^{-1}) was added into 10 mL of CTAB (100 mmol•L^{-1}) water solution, followed by 0.60 mL of ice-cold $NaBH_4$ (10 mmol•L^{-1}) solution was injected, the reaction system turned into a brownish-yellow solution. The resultant solution was completed and kept for about 1 hour before it was used as Au seed for growth Au nanorod. In the typical synthesis of Au nanorod, 5 mL of $HAuCl_4$ (10 mmol•L^{-1}) and 1 mL of $AgNO_3$ (10 mmol•L^{-1}) aqueous solution was mixed with 100 mL of CTAB (100 mmol•L^{-1}) at room temperature under stirring, and then the solution was acidified with 2 mL of HCl (1 mmol•L^{-1}). 0.8 mL of fresh prepared ascorbic acid solution (0.1 mmol•L^{-1}) was added. Finally, 240 μL of Au seed solution was injected into the above growth solution, and then the solution was left in a water bath for 12 hours at 27 ^{o}C. The solution of Au nanorod is purified one time by centrifuging to remove excess CTAB surfactant and then dissolved into water for the next step.

The mesoporous silica coated Au nanorod (defined as $Au_{nanorod}@mSiO_2$) is prepared by the modified single-step coating method.[33] 500 μL of NaOH (0.1 mol•L^{-1}) solution was added into the as-prepared 30 mL of Au nanorod solution. And then, a solution containing 180, 270, 390 and 540 μL of TEOS ethanol solution (20%) were added 3 times interval half an hour under mild stirring at 80 ^{o}C for 6 hours, the $Au_{nanorod}@mSiO_2$ nanostructures with different amorphous silica thickness of 15, 30, 40 and 50 nm were obtained, respectively. The thickness of silica could slightly be increased as the reaction time prolonged. The thickness of silica could be controlled by adjusting the concentration of TEOS and reaction time.

The homogeneous precipitation method was used to coat erbium-doped yttrium oxide on $Au_{nanorod}@mSiO_2$.[25] The solution of $Au_{nanorod}@mSiO_2$ was centrifuged and the precipitation was ultrasonically dispersed in 500 mL of water solution containing $Y(NO_3)_3$ (1 mmol•L^{-1}), $Er(NO_3)_3$ (0.05 mmol•L^{-1}) (Er/Y = 5 at%) and urea (0.25 mol•L^{-1}). The solution was aged at 90 ^{o}C for about 40 min under continuous stirring. The resulting product was centrifuged and washed with water for three times. After calcined at 900 ^{o}C for 1 hour, the $Au_{nanorod}@mSiO_2@Y_2O_3$:Er nanocomposites were obtained.

Characterizations

The X-ray diffraction (XRD) patterns were obtained on an X-ray diffractometer (Bruker, D8 Advance) with Cu radiation ($k\alpha$ = 1.54059 Å). Transmission electron microscopic (TEM) images and high-resolution transmission electron microscopic (HRTEM) images were taken on a FEI F20 operating at 200 kV accelerating voltage. TEM samples were prepared by drop-casting nanoparticles dispersed in DI water onto carbon-coated copper grids. UV/Vis spectra of the products were recorded by a Lambda 40 P UV/Vis spectrometer. The upconversion fluorescence spectrum between 450 nm and 750 nm and the downconversion emission spectra of 1300-1700 nm were respectively measured using the 980 nm laser emission line from Fluorolog-3-Tau Fluorescence spectrometer of Horiba JY company (France) with power is about 130 mW and the detector slit is 1 nm at room temperature. The decay profiles were recorded by an steady state and time resolved fluorescence spectrometer of Edinburgh instruments, R5509 NIR PMT, using laser excitation at 980 nm.

3 Results and discussion

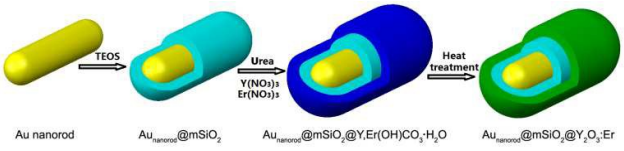

Fig. 1 Schematic illustration of the synthetic procedure for $Au_{nanorod}@mSiO_2@Y_2O_3$:Er nanocomposites.

The strategy to fabricate the nanocomposites is presented in Fig. 1. Firstly, Au nanorod was prepared by the seed-mediated growth approach in the presence of CTAB. Subsequently, the Au nanorod was coated with mesoporous silica to obtain $Au_{nanorod}@mSiO_2$ nanocomposite via base-catalyzed of TEOS. Thirdly, amorphous $Y,Er(OH)CO_3•H_2O$ was deposited on the uniform $Au_{nanorod}@mSiO_2$ nanocomposite through a homogeneous precipitation method. After annealing at high temperature, the $Y,Er(OH)CO_3•H_2O$ layer transferred into Y_2O_3:Er, to realize the formation of the resulting nanocomposite denoted as $Au_{nanorod}@mSiO_2@Y_2O_3$:Er.

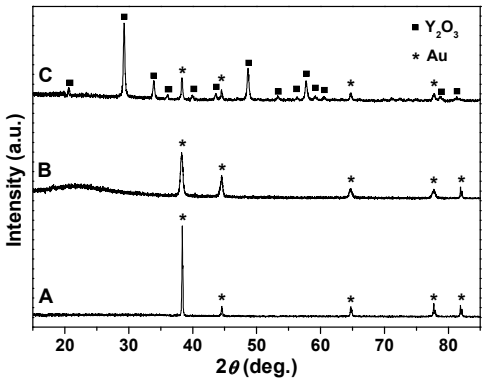

Fig. 2 XRD pattern of (A) Au nanorod; (B) $Au_{nanorod}@15nm\text{-}mSiO_2$ and (C) $Au_{nanorod}@mSiO_2@Y_2O_3$:Er nanoparticles.

The phase composition and crystallinity of the nanoparticles were characterized by XRD. Fig. 2 shows a representative XRD pattern of Au nanorod, $Au_{nanorod}@mSiO_2$, and $Au_{nanorod}@mSiO_2@Y_2O_3$:Er nanocomposites. All of the patterns show Au characteristic peaks marked with stars (Fig. 1A) assigned to (111), (200), (220), (311) and (222) planes of cubic face-centered phase (JCPDS card No. 04-0784). After coating of SiO_2 on the Au nanorod (Fig. 2B), there is a new broad peak between 20 and 25° assigned to the shell of amorphous silica.[22] It is noticed that the intensity of (200) peak in A and B increased after silica coating, which could be due to oxidative etching of the Au nanorod by dissolved O_2.[34,35] In the case of $Au_{nanorod}@mSiO_2@Y_2O_3$:Er nanoparticles (Fig. 2C), except the diffraction peaks of Au, all other diffraction peaks marked with squares can be readily indexed to pure cubic phase of Y_2O_3 (JCPDS card No. 79-1257).

As shown in Fig. 3A, the morphology and size of the Au nanorod was observed by TEM. It can be seen that the rod-like Au nanoparticles with an average length of 53.0 nm and width of 11.0 nm (aspect ratio = 4.8), respectively. The high-resolution TEM image (Fig. 3B) shows that the nanorods are single crystalline by the stacking of (100) planes along the axis. The single crystalline structure of Au seeds and the assistance of Ag (I) lead predominantly to single crystalline gold nanorod with the growth direction along [100] axis.[36] The surfaces of Au nanorods bear a bilayer of CTAB, which could serve as an organic template for the formation of the mesoporous silica layer. Mesoporous silica shell around Au nanorod is fabricated by the method of base-catalyzed hydrolysis and subsequent condensation of TEOS.[33] The silica shell thicknesses ranging from 10 to 50 nm were obtained by varying the reaction time and the amount of TEOS. Fig. 3C and D display the typical TEM images of Au nanorod coated with mesoporous silica shells about 20 and 40 nm thick, respectively. As observed from the enlarged figures, these silica shells possess irregular arranged pore channels as well as open pores. Fig. 3E shows the TEM image of the as-prepared $Au_{nanorod}@mSiO_2@Y_2O_3$:Er nanocomposites. The strong contract between different layers clearly indicates the formation of core-spacer-shell structure. A high-resolution TEM image (Fig. 3F) of the shell layer reveals a polycrystalline feature and the adjacent lattice fringes distance of 0.306 nm, which corresponding to the (222) crystal plane of the cubic phase of Y_2O_3. These results combined with XRD data confirm the detailed structure and composition of the hypothetical nanocomposites in Fig. 1.

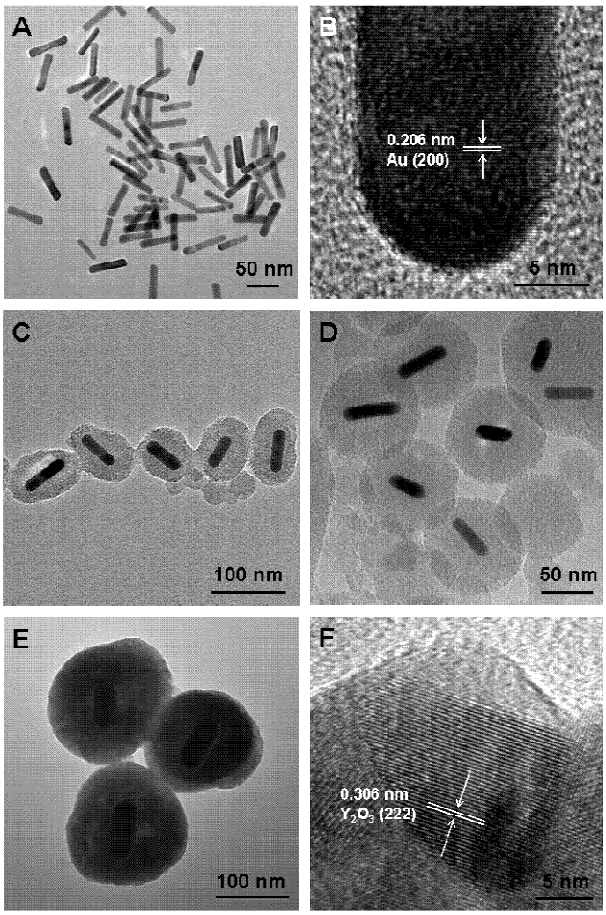

Fig. 3 (A) TEM and (B) high-resolution TEM images of Au nanorod, (C) and (D) TEM images of Au nanorod coated with different SiO_2 thickness of 15 and 40 nm, (E) TEM and (F) high-resolution TEM images of final $Au_{nanorod}@15nm\text{-}mSiO_2@Y_2O_3$:Er nanocomposites, respectively.

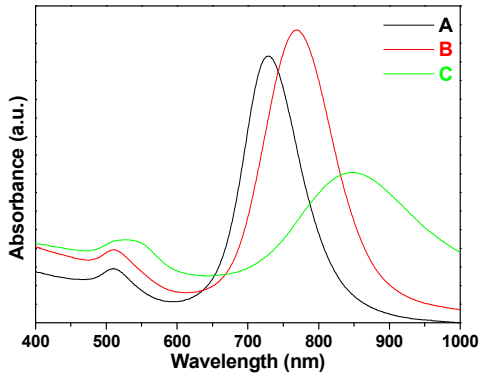

Fig. 4 UV-vis absorption spectra of (A) Au nanorod, (B) $Au_{nanorod}$@15nm-$mSiO_2$, and (C) $Au_{nanorod}$@$mSiO_2$@Y_2O_3:Er nanoparticles, respectively.

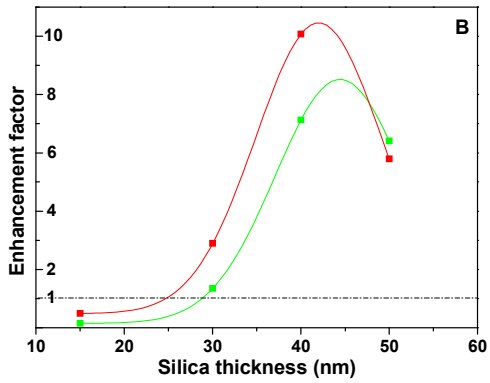

Fig. 5 (A) Upconversion spectra of Y_2O_3:Er and $Au_{nanorod}$@$mSiO_2$@Y_2O_3:Er nanocomposites with different spacer thickness of silica. (B) The plots of enhancement factors of green and red emissions verse silica thickness, respectively. The curves represent Gaussian fit to this data.

Fig. 4 shows the absorption spectra of Au nanorod, $Au_{nanorod}$@$mSiO_2$, and $Au_{nanorod}$@$mSiO_2$@Y_2O_3:Er nanoparticles. The absorption spectrum of Au nanorod (Fig. 4A) has two distinct SPR peaks at 520 and 730 nm associated with the transverse and longitudinal modes, which correspond to free electrons collective oscillations along the transverse and length directions of the nanorod, respectively. After the silica spacer and the Y_2O_3:Er shell coating, the transverse plasmon bands are almost in the same position and the strong longitudinal plasmon band red-shifts to 770 and 850 nm. Because of the SPR related to the dielectric constant of the metal and surrounding dielectric, the wavelength will be red-shift after coating mesoporous silica shell with refractive indexe (n = 1.4585) compared with water (n = 1.3325).[37,38] Also the redshift is strongly dependent on the thickness of mesoporous silica shell (Fig. S1). After yttrium oxide (n = 1.9307) was deposited on the surface of $Au_{nanorod}$@$mSiO_2$ nanoparticles, the absorbance peak will further be red-shift. The absorbance intensity of $Au_{nanorod}$@$mSiO_2$@Y_2O_3:Er nanoparticles is clearly lower than that of Au nanorod and $Au_{nanorod}$@$mSiO_2$ nanoparticles, which could be due to the lower solubility of $Au_{nanorod}$@$mSiO_2$@Y_2O_3:Er nanoparticles in water.

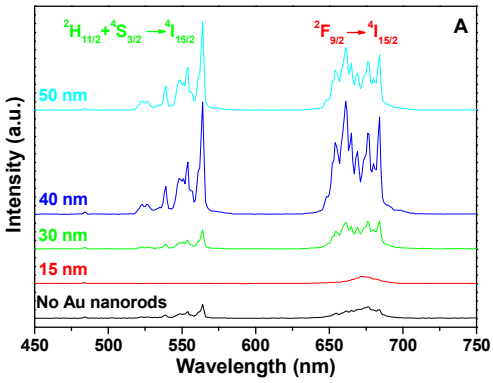

The upconversion fluorescence spectrum of Y_2O_3:Er and $Au_{nanorod}$@$mSiO_2$@Y_2O_3:Er nanocomposites with different spacer thickness of silica were measured under 980 nm laser excitation at room temperature. As shown in Fig. 5A, there are two main characteristic emission bands corresponding to green emission in the 520-570 nm region assigned to the $^2H_{11/2}$ + $^4S_{3/2} \rightarrow {}^4I_{15/2}$ transition and red emission in the 650-700 nm region assigned to the $^4F_{9/2} \rightarrow {}^4I_{15/2}$ transition with Stark-energy splitting for Er^{3+} ions doping in Y_2O_3.[24] It can be seen that the intensity of luminescence strongly depends on the space distance or silica thickness between Au nanorod and Y_2O_3:Er shell. The upconversion fluorescence of the nanocomposites is quenched and then enhanced with increasing the silica thickness from 15 to 50 nm. Therefore, the distance between Au nanorod and Y_2O_3:Er should be optimized to control and enhance the upconversion fluorescence intensity. The strongest enhancement is observed when the silica thickness is 40 nm, resulting in an above 15-fold increase in fluorescence intensity at 660 nm. Fig. 5B displays the plots of green and red fluorescence enhancement factors by dividing integrated fluorescence intensities with silica thickness. The nanocomposite with a silica thickness of about 40 nm shows the strongest enhancement factors of about 10 and 8 for green and red emissions compared to the control of Au-free nanocomposite.

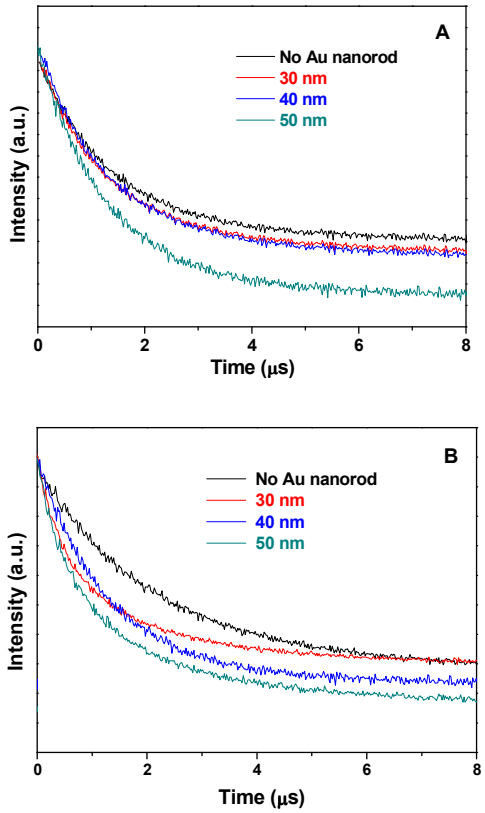

Fig. 6 Up conversion decay curves of Y_2O_3:Er and $Au_{nanorod}@mSiO_2@Y_2O_3$:Er nanocomposites with different spacer thickness of silica at (A) 550 nm and (B) 675 nm, respectively.

It is well known that noble metal Au nanoparticle, nanoshell, and nonorod are particularly useful for the metal-enhanced fluorescence. Au nanorod attracted more attention due to their tunable longitudinal Plasmon absorption in the visible to near infrared spectral region and higher absorption cross-section and light scattering efficiencies than those of nanoshells and nanoparticles.[39] The Au nanorods with various dimensions were synthesized by the seed-mediated growth approach in aqueous CTAB solution. We selected for the demonstration Au rods with aspect ratio of about 5, which shows notable difference from sphericity. CTAB promotes the formation of mesoporous silica with controllable thickness on the Au nanorod surface via hydrolysis and condensation of TEOS by manipulating several parameters, such as the reacted time, temperature, the concentrations of TEOS and CTAB etc.[33] Mesoporous silica-coated Au nanorod are considered to have great potential for cell image, drug or biomolecules delivery, and photothermal cancer therapy. Mesoporous silica on the surface of Au nanorod can also be the spacer to adjusting the fluorescence enhancement or quenching. Here, we construct the $Au_{nanorod}@mSiO_2@Y_2O_3$:Er nanocomposite with core-spacer-shell structure. The result reveals the upconversion fluorescence of Y_2O_3:Er is closely related with the spacer thickness of mesoporous silica. The quenching and enhancement of luminescence comes a result of competition by the distance-dependent mechanism.[13,14] The decay curves of Y_2O_3:Er and $Au_{nanorod}@mSiO_2@Y_2O_3$:Er nanocomposites with different spacer thickness of silica at 550 nm and 675 nm were recorded as shown in Fig. 6. $Au_{nanorod}@mSiO_2@Y_2O_3$:Er nanoparticles exhibit faster radiative decay rates than pure Y_2O_3:Er nanoparticles. Compared with upconversion fluorescence, the down conversion fluorescence intensity and the decay rate at 1550 nm emission have no clear enhancement or quench (Fig. S2 and Fig. S3). It directly proved that the presence of Au nanorod increase the emission rate by surface plasmon coupled emission. When the fluorescence material Y_2O_3:Er is located in close proximity or direct contact to the Au nanorod surface, the fluorescence intensity is reduced dramatically due to the increase of nonradiative energy transfer to Au nanorods.[25,40] With increasing spacer silica thickness, the significant fluorescence enhancement is observed. The origin of the upconversion fluorescence enhancement is due to the enhanced both the incident electromagnetic field intensity and the radiative emission rates from plasmon resonances. Thanks to the two distinct plasmon absorptions of Au nanorod associated with the longitudinal and transverse SPR modes, the plasmon resonances matched very well to the absorption and emission wavelengths in the near IR and visible regions, respectively. Since the Au nanorod has higher absorption cross-section and relatively light scattering efficiencies, the SPR peak of $Au_{nanorod}@mSiO_2@Y_2O_3$:Er nanocomposite was shifted to 850 nm, which is near the excitation light at 980 nm. It means the presence of Au nanorod can locally concentrate the incident field and enhance absorption, improving reception. Thus, the effective excitation flux is improved by the local filed enhancement, which leads to an enhancement of the upconversion emission. The future efforts will further modify the aspect ratio of Au nanorod and allow us to tune the plasmon peak and perform a systematic investigation of this aspect. When the plasmon resonance matched to the emission wavelengths, the upconversion emission will be enhanced by increasing radiative decay rates via the surface Plasmon-coupled emission. Under the 980 nm laser excitation, the Er^{3+} ions are excited first from the ground state $^4I_{15/2}$ level to the $^2H_{11/2}$ level and then from $^2H_{11/2}$ to $^4F_{7/2}$ level via a two photons process. Subsequently, the electrons in the $^4F_{7/2}$ level of Er^{3+} ions decay nonradiatively to the $^2H_{11/2}$, $^4S_{3/2}$, or $^4F_{9/2}$ level and the green and red emissions are observed via energy-transfer upconversion and excited-state absorption processes.[41] The Er-density of states maybe changed due to the presence of Au nanrods, and the further experiment and simulation need to perform. In the case of the nanocomposites with Au or Ag cores and Er-doped or Er,Yb co-doped oxide shells involved silica spacer layers, they all exhibited the enhancement of upconversion fluorescence.[25,26] The green emission was preferentially enhanced more than the red emission due to the better spectral overlap with the Plasmon resonance of nanoparticles was confined to the visible region at around 500-550 nm. As for the $Au_{nanorod}@mSiO_2@Y_2O_3$:Er nanocomposite in our case, there is still strong absorption in the red region compared with the green region (Fig. 4). The upconversion red

emission also shows sensitive enhancement with a maximum enhancement factor of above 10 at an optimal silica spacer thickness of 40 nm. Hence, the plasmon resonances simultaneously matched to absorption and emission lead to a rather great enhancement of red and green upconversion in comparison with those in previous reports.[25,26]

Conclusions

In summary, we have fabricated well-defined $Au_{nanorod}$@$mSiO_2$@Y_2O_3:Er nanocomposites with Au nanorod core, Y_2O_3:Er shell, and mesoporous silica as spacer. The thickness of silica layer could be simply controlled by varying the reaction time and the amount of TEOS. Thanks to the two distinct plasmon absorptions of Au nanorod associated with the longitudinal and transverse SPR modes, the plasmon resonances matched very well to the absorption and emission wavelengths in the near IR and visible regions, respectively. The strongest enhancement is observed when the optimized silica thickness is around 40 nm, resulting in about 10- and 8-fold enhancement for green and red emissions compared to the control of Au-free nanocomposite, respectively. Besides the enhanced upconversion fluorescence, the prepared nanocomposites with unique properties and functions offered by Au nanorod and mesoporous silica structure will expected to be useful in photothermal therapy, drug delivery, medical diagnostics and therapy.[42-44]

Acknowledgements

This work was financially supported by the Science Research Foundation of Northwest University (No. 13NW121) and the Education Commission of Shaanxi Province (No. 2014JQ6223, 12JS114, and 14JS092).

Notes and references

1 F. Auzel, *Chem. Rev.*, 2004, **104**, 139-173.
2 M. Haase and H. Schafer, *Angew. Chem. Int. Ed.*, 2011, **50**, 5808-5829.
3 J. Zhou, Q. Liu, W. Feng, Y. Sun and F. Li, *Chem. Rev.*, 2015, **115**, 395-465.
4 G. Liu, *Chem. Soc. Rev.*, 2015, **44**, 1635-1652.
5 C. Bouzigues, T. Gacoin and A. Alexandrou, *ACS Nano*, 2011, **5**, 8488-8505.
6 H. Dong, L. Sun and C. Yan, *Chem. Soc. Rev.*, 2015, **44**, 1608-1634.
7 G. Chen, H. Qiu, P. N. Prasad and X. Chen, *Chem. Rev.*, 2014, **114**, 5161-5214.
8 S. Han, R. Deng, X. Xie and X. Liu, *Angew. Chem. Int. Ed.*, 2014, **53**, 11702-11715.
9 G. Chen, H. Agren, T. Y. Ohulchanskyy and P. N. Prasad, *Chem. Soc. Rev.*, 2015, **44**, 1680-1713.
10 V. Giannini, A. I. Fernandez-Dominguez, S. C. Heck and S. A. Maier, *Chem. Rev.*, 2011, **111**, 3888-3912.
11 X. Li, F. Zhang and D. Zhao, *Nano Today*, 2013, **8**, 643-676.
12 C. D. Geddes and J. R. Lakowicz, *J. Fluoresc.*, 2002, **12**, 121-129.
13 D. M. Wu, A. Garcia-Etxarri, A. Salleo and J. A. Dionne, *J. Phys. Chem. Lett.*, 2014, **5**, 4020-4031.
14 W. Park, D. Lu and S. Ahn, *Chem. Soc. Rev.*, 2015, **44**, 2940-2962.
15 P. Reineck, D. Gomez, S. H. Ng, M. Karg, T. Bell, P. Mulvaney and U. Bach, *ACS Nano*, 2013, **7**, 6636-6648.
16 C. Zhang and J. Y. Lee, *J. Phys. Chem. C*, 2013, **117**, 15253-15259.
17 N. S. Abadeer, M. R. Brennan, W. L. Wilson and C. J. Murphy, *ACS Nano*, 2014, **8**, 8392-8406.
18 D. Yin, C. Wang, J. Ouyang, X. Zhang, Z. Jiao, Y. Feng, K. Song, B. Liu, X. Cao, L. Zhang, Y. Han and M. Wu, *ACS Appl. Mater. Interfaces*, 2014, **6**, 18480-18488.
19 W. Xu, X. Min, X. Chen, Y. Zhu, P. Zhou, S. Cui, S. Xu, L. Tao and H. Song, *Sci. Rep-UK*, 2014, **4**, 5087.
20 S. Zhang, L. Sun, H. Tian, Y. Liu, J. Wang and C. Yan, *Chem. Commun.*, 2009, 2547-2549.
21 W. Feng, L. Sun and C. Yan, *Chem. Commun.*, 2009, 4393-4395.
22 Z. Li, L. Wang, Z. Wang, X. Liu and Y. Xiong, *J. Phys. Chem. C*, 2011, **115**, 3291-3296.
23 T. Som and B. Karmakar, *J. Appl. Phys.*, 2009, **105**, 013102.
24 J. A. Capobianco, F. Vetrone and J. C. Boyer, *J. Phys. Chem. B*, 2002, **106**, 1181-1187.
25 F. Zhang, G. B. Braun, Y. Shi, Y. Zhang, X. Sun, N. O. Reich, D. Zhao and G. Stucky, *J. Am. Chem. Soc.*, 2010, **132**, 2850-2851.
26 W. Ge, X. R. Zhan, M. Liu, Z. W. Lei, R. J. Knize and Y. Lu, *Theranostics*, 2013, **3**, 282-288.
27 H. Zhang, Y. Li, I. A. Ivanov, Y. Qu, Y. Huang and X. Duan, *Angew. Chem. Int. Ed.*, 2010, **49**, 2865-2868.
28 A. Priyam, N. M Idris and Y. Zhang, *J. Mater. Chem.*, 2012, **22**, 960-965.
29 P. K. Jain, K. S. Lee, I. H. El-Sayed and M. A. El-Sayed, *J. Phys. Chem. B*, 2006, **110**, 7238-7248.
30 S. Liu, L. Huang, J. Li, C. Wang, Q. Li, H. Xu, H. Guo, Z. Meng, Z. Shi and Z. Li, *J. Phys. Chem. C*, 2013, **117**, 10636-10642.
31 Q. Luu, A. Hor, J. Fisher, R. B. Anderson, S. Liu, T. Luk, H. P. Paudel, M. F. Baroughi, P. S. May and S. Smith, *J. Phys. Chem. C*, 2014, **118**, 3251-3257.
32 B. Nikoobakht and M. A. El-Sayed, *Chem. Mater.*, 2003, **15**, 1957-1962.
33 I. Gorelikov and N. Matsuura, *Nano Lett.*, 2008, **8**, 369-373.
34 R. Long, S. Zhou, B. J. Wiley and Y. Xiong, *Chem. Soc. Rev.*, 2014, **43**, 6288-6310.
35 T.-S. Deng, J. E. S. van der Hoeven, A. O. Yalcin, H. W. Zandbergen, M. A. van Huis and A. van Blaaderen, *Chem. Mater.*, 2015, **27**, 7196-7203.
36 M. Liu and P. Guyot-Sionnest, *J. Phys. Chem. B*, 2005, **109**, 22192-22200.
37 L. M. Liz-Marzan, M. Giersig and P. Mulvaney, *Langmuir*, 1996, **12**, 4329-4335.
38 http://refractiveindex.info/
39 R. Bardhan, N. K. Grady, J. R. Cole, A. Joshi and N. J. Halas, *ACS Nano*, 2009, **3**, 744-752.
40 Y. Song, G. Liu, X. Dong, J. Wang, W. Yu and J. Li, *RSC Adv.*, 2014, **4**, 62802-62808.
41 Y. Song, G. Liu, X. Dong, J. Wang, W. Yu and J. Li, *J. Phys. Chem. C*, 2015, **119**, 18527-18536.
42 B. Dong, S. Xu, J. Sun, S. Bi, D. Li, X. Bai, Y. Wang, L. Wang and H. Song, *J. Mater. Chem.*, 2011, **21**, 6193-6200.
43 Z. Jiang, B. Dong, B. Chen, J. Wang, L. Xu, S. Zhang and H. Song, *Small*, 2013, **9**, 604-612.
44 X. Chen, W. Xu, L. Zhang, X. Bai, S. Cui, D. Zhou, Z. Yin, H. Song and D. -H. Kim, *Adv. Funct. Mater.*, 2015, **25**, 5462-5471.

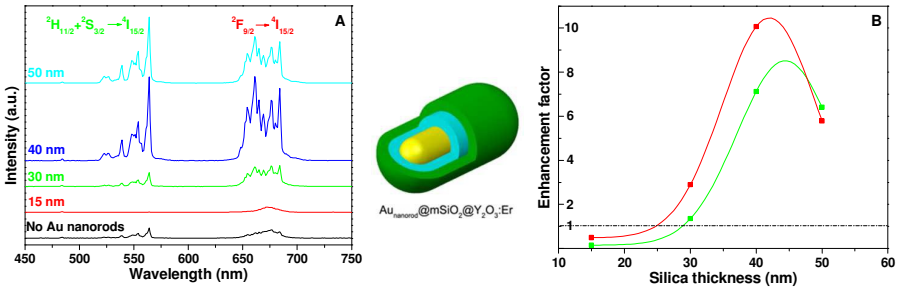

We fabricated the well-defined $Au_{nanorod}@mSiO_2@Y_2O_3$:Er nanocomposites with about 10- and 8-fold strongest upconversion enhancement for green and red emissions, respectively.